Annals of Biomedical Engineering, Vol. 35, No. 8, August 2007 *(© 2007)* pp. 1425–1443
DOI: 10.1007/s10439-007-9299-5

A Nonlinear Model of Cardiac Autonomic Control in Obstructive Sleep Apnea Syndrome

JAVIER A. JO,[1,3] ANNA BLASI,[1] EDWIN M. VALLADARES,[1] RICARDO JUAREZ,[2] AHMET BAYDUR,[2] and MICHAEL C. K. KHOO [1]

[1]Department of Biomedical Engineering, OHE-500, University of Southern California, Los Angeles, CA, 90080-1451 USA; [2]Department of Medicine, University of Southern California, Los Angeles, CA, USA; and [3]Department of Biomedical Engineering, Texas A&M University, College Station, TX, USA

(Received 21 November 2006; accepted 23 March 2007; published online 6 April 2007)

Abstract—Using the Volterra–Wiener approach, we employed a minimal model to quantitatively characterize the linear and nonlinear effects of respiration (RCC) and arterial blood pressure (ABR) on heart rate variability (HRV) in normal controls and subjects with moderate-to-severe obstructive sleep apnea syndrome (OSAS). Respiration, R–R interval (RRI), blood pressure (BP) and other polysomnographic variables were recorded in eight normal controls and nine OSAS subjects in wakefulness, Stage 2 and rapid eye-movement sleep. To increase respiratory and cardiovascular variability, a preprogrammed ventilator delivered randomly timed inspiratory pressures that were superimposed on a baseline continuous positive airway pressure. Except for lower resting RRI in OSAS subjects, summary statistical measures of RRI and BP and their variabilities were similar in controls and OSAS. In contrast, RCC and ABR gains were significantly lower in OSAS. Nonlinear ABR gain and the interaction between respiration and blood pressure in modulating RRI were substantially reduced in OSAS. ABR gain increased during sleep in controls but remained unchanged in OSAS. These findings suggest that normotensive OSAS subjects have impaired daytime parasympathetic and sympathetic function. Nonlinear minimal modeling of HRV provides a useful, insightful, and comprehensive approach for the detection and assessment of abnormal autonomic function in OSAS.

Keywords—Autonomic nervous system, Heart rate variability, Baroreflex, Respiratory sinus arrhythmia, Volterra–Wiener model, Minimal model, Closed-loop control.

INTRODUCTION

Obstructive sleep apnea syndrome (OSAS) is characterized by repeated episodes of upper airway occlusion during sleep. Each occlusion episode results in increasing asphyxia until transient arousal restores upper airway patency. The cardiovascular consequences of these events are profound, and chronic exposure to obstructive apnea constitutes an independent risk factor for systemic hypertension, heart failure, myocardial infarction, and stroke.[5,32,39] Abnormal autonomic control has been suggested as the common factor linking OSAS to these cardiovascular diseases.[21,34,37]

Recently, we introduced a new noninvasive approach for quantitatively assessing autonomic function in OSAS under different sleep–wake states. This method is based on a closed-loop minimal model of heart rate variability (HRV) that assumes HRV to be generated via two functional mechanisms: direct respiratory–cardiac coupling and the arterial baroreflex.[17] This model was able to capture the most salient features of the cardiorespiratory dynamics under study, but was unable to account for a significant residual fraction of the total variance, particularly dynamics at frequencies below 0.1 Hz. We hypothesize that this residual variance was the consequence of the assumption of linear dynamics in our original model, and that the discrepancy can be largely eliminated by extending the model to incorporate simple nonlinearities in and interactions between the model inputs.

For small fluctuations about a mean operating point, linear system identification methods provide a convenient and effective means for characterizing a physiological system. However, in many situations, spontaneous or induced physiological fluctuations can be large enough that nonlinear dynamic effects cannot be ignored. Nonlinear dynamics can lead to phenomena such as limit cycles, threshold, and saturation effects, which are commonly observed in physiological systems.[38] Experimental studies have also demonstrated nonlinear interactions between the sympathetic

Address correspondence to Michael C. K. Khoo, Department of Biomedical Engineering, OHE-500, University of Southern California, Los Angeles, CA, 90080-1451 USA. Electronic mail: khoo@bmsr.usc.edu

Supported by NIH Grants HL-58725, EB-001978, and M01 RR-43

and parasympathetic nervous system with respect to heart rate control.[14,23] As such, several recent studies have employed nonlinear dynamical theory and fractal analysis to characterize HRV.[24] Fractal analysis has been shown to be useful for purposes of risk stratification in patients with impaired left ventricular function following myocardial infarction, providing better prediction of mortality in this patient population.[16] However, one limitation of these univariate analyses is that they provide information of only the net effects of the many influences that give rise to HRV. In contrast, the "input–output" minimal model approach we have adopted yields greater insight into how the main physiological mechanisms that contribute to HRV are altered in OSAS. As well, this kind of model can be readily adapted for investigating conditions under which rapidly changing dynamics may be important, such as during transient state changes during sleep.[3]

The approach outlined in this paper employs a second-order nonlinear time-invariant dual-input representation, based on the Laguerre expansion technique (LET) for Volterra–Wiener kernel estimation.[26] The advantages of this technique and its applications to modeling renal blood pressure-flow properties as a single-input single-output system were demonstrated by Marmarelis and colleagues.[7,27] The extension of the Laguerre expansion technique to the estimation of a dual-input HRV model was introduced by Chon *et al.*[8] In this study, we propose a model similar in structure to Chon's to determine how respiratory–cardiac coupling and the baroreflex control of heart rate are altered by OSAS during wake and sleep.

In summary, the specific objectives of this study are: (a) to quantify the nonlinear dynamics involved on the modulation of HRV by changes in respiration and blood pressure; (b) to determine the significance of these nonlinear interactions on the overall variability of the heart rate; and (c) to assess how these nonlinear dynamics are affected by OSAS and changes in wake–sleep state.

METHODS

Experimental Protocol and Instrumentation

Nine untreated patients with moderate-to-severe OSAS (apnea-hypopnea index = 44.1 ± 2.8 h^{-1}) and eight normal controls underwent overnight polysomnography, preceded by application of the test protocol (described below) during wakefulness. Age was not significantly different between the two groups; however, body-mass index was significantly higher in the OSAS patients ($p < 0.05$). All subjects were normotensive and were free of diabetes, significant cardiac arrhythmia, congestive heart failure, and lung disease. Informed consent was obtained prior to each study. The study protocol was approved by the USC Institutional Review Board.

Arterial blood pressure (ABP) was monitored continuously from one wrist using a noninvasive arterial tonometer (Model 7000, Colin Medical Instruments, San Antonio, TX). Electrocardiogram (ECG), arterial oxygen saturation (S_{aO_2}), central and occipital electroencephalogram, chin electromyogram, left and right electrooculogram, and nasal thermistor were also monitored. All signals were sampled at 200 Hz.

Each subject was connected via nasal mask to a computer-controlled bilevel pressure ventilator (S/T-D 30, Respironics, Pittsburgh, PA). Measurements of mask pressure and airflow were obtained from the detachable control panel of the S/T-D ventilator. Airflow was electronically integrated in both inspiratory and expiratory phases to obtain the instantaneous lung volume (V_t) relative to passive functional residual capacity. We determined in initial tests that the tidal volumes derived from the ventilator volume monitor were highly correlated ($r > 0.97$, $p = 0.0001$) with corresponding readings obtained from a reference pneumotachometer (Model 3700, Hans Rudolph, Kansas City, MO). A chinstrap was used to keep the mouth closed during sleep, preventing leakage or inspiration through the mouth. Continuous monitoring of mask pressure enabled the detection of abrupt or unusual changes in baseline pressure that could indicate leaks through the mouth.

A minimal continuous positive airway pressure (CPAP) of 2–3 cm H_2O was applied during wakefulness in the control group in order to overcome the additional resistance to breathing presented by the mask and respiratory apparatus. In the OSAS patients, the levels of CPAP applied ranged from 8 to 15 cm H_2O, depending on what was necessary to eliminate obstructive apnea and significant hypopnea during sleep. Obstructive apneas were identified as episodes of zero airflow lasting 10 s or more, and hypopneas as periods >10 s duration in which the nasal thermistor signal was reduced to $<50\%$ of its magnitude during unobstructed breathing and S_{aO_2} decreased by $>4\%$. Thus, in the OSAS subjects, obstructive apneas and hypopneas were prevented from occurring throughout the night.

During the 10-min test protocol, the ventilator was set to assist-control, bilevel ventilation mode. Under this condition, the subject was allowed to breathe at his own respiratory rate, but the inspiratory pressure was switched randomly breath-to-breath between the CPAP level and CPAP + 5 cm H_2O. Expiratory pressure was kept constant at the CPAP level. Using this experimental setup, tidal volume was modulated breath-to-breath without the need for voluntary

control by the subject. This test protocol, which allowed the ventilatory pattern of each subject to contain a broadened spectrum of frequencies, was designed to enhance the accuracy and reliability of subsequent parameter estimation from the recorded data.[20]

Following one or two trials to minimize subject anxiety during wakefulness, the test protocol was applied at least three times in each sleep–wake state. Test sequences which elicited arousals or outright awakening were terminated, and the protocol was not repeated until the subject returned to a stable sleep state. Sleep stages were scored according to conventional criteria.[30]

Data Analysis

From each 10-min test segment, R–R intervals (RRI), and systolic blood pressure (SBP) and diastolic blood pressure (DBP) values were estimated beat-to-beat from the ECG and ABP signals and resampled at 2 Hz using the Berger algorithm.[2] Very low-frequency oscillatory behavior or baseline drift was observed in some of the datasets. These ultra low-frequency nonstationarities were removed by detrending the datasets prior to applying spectral analysis and modeling.

The Model

RRI, V_t, and SBP were assumed to be interrelated through a closed-loop control scheme consistent with the underlying physiology, as had been previously proposed.[1,29] We assumed that respiration influences RRI directly through autonomic respiratory–cardiac coupling (RCC). The latter is believed to be the result of central respiratory entrainment of the cardiovagal motorneurons in the medulla as well as vagal feedback from the pulmonary stretch receptors.[10] Respiration also affects RRI indirectly through changes in intrathoracic pressure, which are translated into changes in blood pressure that subsequently act on the arterial baroreflex (ABR). The totality of these respiratory influences on HRV constitutes what is commonly termed "respiratory sinus arrhythmia."[10] The "closed-loop" nature of the control scheme derives from the fact that changes in RRI lead to changes in cardiac output, which, in turn, influence blood pressure. Apart from intrathoracic pressure changes and changes in cardiac output, fluctuations in blood pressure can also arise from other sources of spontaneous variability, such as sympathetically driven variations in peripheral vascular resistance.

The focus of this study was limited to the portion of the closed-loop model that accounts for HRV. The model, illustrated schematically in Fig. 1, assumes that fluctuations in heart rate are produced through six functional mechanisms. The first five sources correspond to autonomic-mediated mechanisms involved in the variability of the heart rate: a component with linear dynamics representing the neural coupling of respiration and heart rate (*Hx*); a linear arterial baroreflex (ABR) component (*Hu*); two nonlinear compartments describing the second-order effects of respiration (*Hxx*) and blood pressure (*Huu*) on heart rate; and a third nonlinear compartment characterizing multiplicative interaction of respiration and blood pressure on heart rate (*Hxu*). The last source (W_{RRI}) encompasses all other influences not explained by the other linear and nonlinear components.

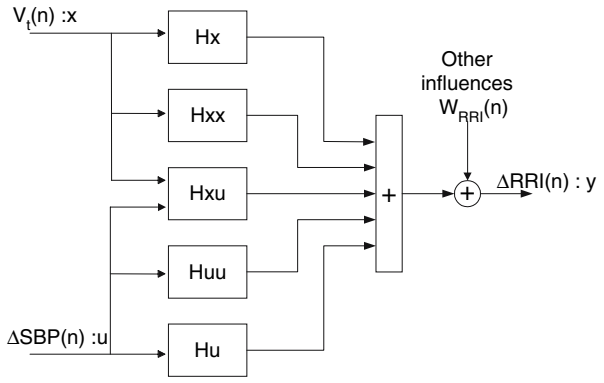

FIGURE 1. Schematic block diagram of the dual-input second-order model of HRV. Fluctuations in RRI (HRV) are assumed to be produced by: a neural coupling of respiration and RRI (*Hx*); an arterial baroreflex component (*Hu*); nonlinear (second-order) effects of respiration (*Hxx*) and blood pressure (*Huu*) on RRI; and nonlinear (second-order) interaction of respiration and blood pressure on RRI (*Hxu*). $W_{\mathrm{RRI}}(n)$ encompasses all other influences not explained by the model.

The nonlinear dynamic relationship between the two inputs $x(t)$ (V_t) and $u(t)$ (ΔSBP) , and the system output $y(t)$ (ΔRRI) was represented by a second-order time-invariant Volterra–Wiener model, represented by the following equation:

$$\begin{aligned} y(t) = & T\sum_{\tau=0}^{M} k_x(\tau)x(t-\tau-D_x) + T\sum_{\tau=0}^{M} k_u(\tau)x(t-\tau-D_u) \\ & + T^2\sum_{\tau_1=0}^{M}\sum_{\tau_2=0}^{M} k_{xx}(\tau_1,\tau_2)x(t-\tau_1-D_x)x(t-\tau_2-D_x) \\ & + T^2\sum_{\tau_1=0}^{M}\sum_{\tau_2=0}^{M} k_{uu}(\tau_1,\tau_2)u(t-\tau_1-D_u)u(t-\tau_2-D_u) \\ & + T^2\sum_{\tau_1=0}^{M}\sum_{\tau_2=0}^{M} k_{xu}(\tau_1,\tau_2)x(t-\tau_1-D_x)u(t-\tau_2-D_u) \\ & + W_{\mathrm{RRI}}(t) \end{aligned} \tag{1}$$

The above equation assumes a *discrete* time base t with sampling interval T (= 0.5 s). The parameter M determines the extent of the system memory. The linear kernels k_x and k_u represent the linear contribution to

the output of each single signal. The nonlinear self-kernels k_{xx} and k_{uu} represent the quadratic contribution of each input signals. The cross-kernel k_{xu} describes the effect on the output resulting from the second-order nonlinear interaction of the two input signals. The second-order self-kernels are symmetric functions of their arguments and the second-order cross-kernels are asymmetric functions of their arguments.

In Eq. (1), D_x and D_u are the delays between the output (ΔRRI) and the two inputs (ΔV and ΔSBP , respectively) associated with the corresponding mechanisms; and the signal $W_{\mathrm{RRI}}(t)$ represents the variability of RRI not explained by the model. Causality constraints were also imposed upon the model to account for the closed-loop structure of the baroreflexes. A delay of at least $D_u = 0.5$ s was inserted in the baroreflex dynamics. Previous studies have suggested that changes in heart rate are synchronous with neural respiration but precedes mechanical inspiration.[1,8,17,29] Therefore, the nonlinear model was allowed to adopt negative values of the delay D_x. In order to accommodate this effect, the RRI signal was delayed before the estimation. Shifting the estimated RCC first- and second-order kernels back in time later compensated for this negative delay.

A linear version of the model (which includes only the first two summations in Eq. (1) was also estimated, in order to determine the improvement in predictive ability of the model when the nonlinear contributions are taken into account. A description of the Laguerre expansion of the kernels technique applied in the present work for the estimation of our proposed nonlinear model is presented in the following section.

It is imperative to note that the system under study operates in a closed-loop, so that changes in heart rate can subsequently affect SBP through changes in cardiac output. In general, this condition, in which the model input is dependent on its output, can lead to erroneous parameter estimates when conventional analysis techniques are employed. To circumvent this problem, we formulated the model equations in the time domain so that "causality" constraints could be imposed: i.e., the model output was constrained mathematically to be dependent on only past values of the inputs. Previous studies have employed similar methodologies that essentially allow the closed loop to be "opened" computationally.[1,29]

Model Estimation and Optimization

The traditional and most straightforward technique for multiple-input system kernel estimation has been the cross-correlation technique proposed by Lee and Schetzen,[22] which performs a Gram–Schmidt orthogonalization of the Volterra series expansion with respect to Gaussian white noise. The simplicity of this method has facilitated its application to a wide variety of physiological systems. However, it requires long data records, strict whiteness of the input, and a heavy computational burden associated with the estimation of higher-order kernels. An improved version of the algorithm based on the Laguerre expansion of the kernels[26] alleviates most of the deficiencies inherent in the cross-correlation technique. In particular, the Laguerre expansion technique (LET) does not require strict whiteness of the input since Gram–Schmidt orthogonalization with respect to Gaussian white noise is not utilized. Instead, unknown Laguerre expansion coefficients are estimated using least-squares minimization. This leads to increased estimation accuracy in the presence of noise, reduces the requirement for long data records, and allows accurate kernel estimation when the input deviates from the theoretical requirement for white-noise stimuli.[26] The Laguerre functions have been suggested as an appropriate orthonormal basis, owing to their built-in exponential term that makes them suitable for modeling physical systems with asymptotically exponential relaxation dynamics.[26] The Laguerre expansion technique uses the orthonormal set of discrete time Laguerre functions $b_j(\tau)$ to discretize and expand the system kernels of the second-order Volterra model as follows:

$$\begin{aligned} k_1(\tau) &= \sum_{jx=1}^{S1} c_{x1}(j_x) b_{jx}(\tau) + \sum_{ju=1}^{S2} c_{u1}(j_u) b_{ju}(\tau) \\ k_2(\tau_1,\tau_2) &= \sum_{jx1=1}^{S1}\sum_{jx2=1}^{S1} c_{x2}(j_{x1},j_{x2}) b_{jx1}(\tau_1) b_{jx2}(\tau_2) \\ &\quad + \sum_{ju1=1}^{S2}\sum_{ju2=1}^{S2} c_{u2}(j_{u1},j_{u2}) b_{ju1}(\tau_1) b_{ju2}(\tau_2) \\ &\quad + \sum_{jx=1}^{S1}\sum_{ju=1}^{S2} c_{xu}(j_x,j_u) b_{jx}(\tau_1) b_{ju}(\tau_2) \end{aligned} \tag{2}$$

In Eq. (2), $\{c_{x1}(\cdot), c_{x2}(\cdot), c_{u1}(\cdot), c_{u2}(\cdot), c_{xu}(\cdot)\}$ are the sets of the unknown expansion coefficients, which are to be estimated from the input–output data; $b_j(\tau)$ denotes the jth order orthonormal discrete time Laguerre function; $S1$ and $S2$ are the number of Laguerre functions used to model both the linear and nonlinear dynamics corresponding to the interaction between the two inputs and the output. The Laguerre functions basis is defined as:

$$\begin{aligned} b_j(\tau) =& \alpha^{(\tau-j)/2}(1-\alpha)^{1/2} \sum_{k=0}^{j} (-1)^k \binom{\tau}{k}\binom{j}{k} \\ & \times \alpha^{j-k}(1-\alpha)^k, \quad \tau \geq 0 \end{aligned} \tag{3}$$

In a more efficient implementation, $b_j(\tau)$ can be computed recursively as follows:

$$b_0(\tau) = \sqrt{\alpha^{\tau}(1-\alpha)}$$
$$b_j(\tau) = \sqrt{\alpha}b_j(\tau-1) + \sqrt{\alpha}b_{j-1}(\tau) - b_{j-1}(\tau-1), \quad j>0 \tag{4}$$

The parameter ($0 < \alpha < 1$) determines the rate of exponential decline of the Laguerre functions. This parameter is selected based on the kernel memory length and the number of Laguerre functions used for expansion, so that all the functions decline sufficiently close to zero by the end of the kernel.[26] The memory length of the kernels was fixed to 50 s (100 samples), based on our previous results obtained from applying a linear model to the same data sets.[17,18] By inserting Eq. (2) into Eq. (1), the second-order Volterra model thus becomes:

$$\begin{aligned} y(t) = &\sum_{jx=1}^{S1} c_{x1}(j_x)v_{jx}(t) + \sum_{ju=1}^{S2} c_{u1}(j_u)w_{ju}(t) \\ &+ \sum_{jx1=1}^{S1}\sum_{jx2=1}^{S1} c_{x2}(j_{x1},j_{x2})v_{jx1}(t)v_{jx2}(t) \\ &+ \sum_{ju1=1}^{S2}\sum_{ju2=1}^{S2} c_{u2}(j_{u1},j_{u2})w_{ju1}(t)w_{ju2}(t) \\ &+ \sum_{jx=1}^{S1}\sum_{ju=1}^{S2} c_{xu}(j_x,j_u)v_{jx}(t)w_{ju}(t) \end{aligned} \tag{5}$$

where $v_j(t)$ and $w_j(t)$ are the discrete convolutions of the inputs with Laguerre functions and denoted as the "key variables":

$$\begin{aligned} v_j(t) &= T\sum_{\tau=0}^{M} b_j(\tau)x(t-\tau-D_x) \\ w_j(t) &= T\sum_{\tau=0}^{M} b_j(\tau)u(t-\tau-D_u) \end{aligned} \tag{6}$$

The unknown expansion coefficients $\{c_{x1}(\cdot), c_{x2}(\cdot), c_{u1}(\cdot), c_{u2}(\cdot), c_{xu}(\cdot)\}$ can be estimated by generalized least-square fitting using the time-series $y(t)$, $v_j(t)$ and $w_j(t)$.

To select the model with the minimum number of parameters (minimal number of Laguerre functions, and hence, expansion coefficients) that would best fit the observations, the following optimization procedure was applied. For a given set of number of Laguerre functions $\{S1, S2\}$ and delays $\{D_x, D_u\}$, the expansion coefficients were calculated for all combinations of $\{S1, S2\}$ ranging from 1 to 7, with D_x ranging from −2 to 1 s (corresponding to the RSA delay) and D_u from 0.5 to 2 s (corresponding to the ABR delay). The "optimal model" was selected by searching for the *global minimum of the minimum description length*[31] over the entire grid of values for $\{S1, S2\}$ and the delays $\{D_x, D_u\}$. Model adequacy was checked by testing for whiteness of the residuals and the lack of correlation between the corresponding inputs and residuals.[33] The normalized mean squared error (NMSE) and coherence function served as indicators of the prediction accuracy. The optimization procedure was performed for every set of data.

Once the Laguerre expansion coefficients for the optimal candidate model were estimated, the linear impulse response corresponding to the two mechanisms represented in our model (RCC and ABR) were related to the linear self-kernels as follows:

$$\begin{aligned} h_{\mathrm{RCC}}(t) &= k_x(t) = \sum_{j=0}^{S1} c_{x1}(j)b_j(t) \\ h_{\mathrm{ABR}}(t) &= k_u(t) = \sum_{j=0}^{S2} c_{u1}(j)b_j(t) \end{aligned} \tag{7}$$

Similarly, the second-order self- and cross-kernels were estimated from the expansion coefficients as follows:

$$\begin{aligned} k_{xx}(\tau_1,\tau_2) &= \sum_{jx1=1}^{S1}\sum_{jx2=1}^{S1} c_{x2}(j_{x1},j_{x2})b_{jx1}(\tau_1)b_{jx2}(\tau_2) \\ k_{uu}(\tau_1,\tau_2) &= \sum_{ju1=1}^{S2}\sum_{ju2=1}^{S2} c_{u2}(j_{u1},j_{u2})b_{ju1}(\tau_1)b_{ju2}(\tau_2) \\ k_{xu}(\tau_1,\tau_2) &= \sum_{jx=1}^{S1}\sum_{ju=1}^{S2} c_{xu}(j_x,j_u)b_{jx}(\tau_1)b_{ju}(\tau_2) \end{aligned} \tag{8}$$

The corresponding linear version of the models were also optimized using the same procedure described above, but allowing the number of Laguerre functions employed $\{S1, S2\}$ to range from 1 to 15.

Statistical Analysis

To facilitate statistical comparison, compact descriptors were derived from the model impulse responses. One of these is the impulse response magnitude (IRM) or the difference between the maximum and minimum values of linear kernel. In order to compare the nonlinear dynamics of the system, the Kernel Magnitude (*KM*), defined as the difference between maximum and minimum values of the estimated second-order kernels was computed.

Each estimated parameter was subjected to two-way repeated-measures analysis of variance (subject group × sleep–wake state). *Post-hoc* multiple pairwise

comparisons (Student–Newmans–Keuls test) were carried out if statistical significance was indicated.

Physiological Interpretation of Nonlinear HRV Dynamics

One of the limitations of the Volterra–Wiener approach to system identification is that the higher-order kernels do not readily lend themselves to physiological interpretation. To derive greater insight into the dynamics characterized by the estimated second-order kernels and what they mean in terms of the underlying physiological mechanisms, we performed the following simulations.

It has been previously observed that the frequency response relating respiration to RRI is dependent on tidal volume.[15] In order to test the hypothesis that the second-order RCC component of our model reflects this observation, we convolved the average *Hx* and *Hxx* with a chirp signal (frequency range 1–45 cycles/min) of fixed amplitude of V_T liters. The FFT of the estimated RRI response was then derived to represent the frequency response of the RCC component at the given tidal volume of V_T liters. The simulations were repeated for various V_T values (0.5, 1, 2, and 3 L). We anticipated that without the *Hxx* component, the frequency response (normalized to the tidal volume level) would be independent of V_T. However, with *Hxx*, there should be V_T dependence, so that as V_T increases, RCC gain increases.

It is also well established that the steady-state ABR response is not linear, showing saturation at higher blood pressure levels. In order to test the hypothesis that the second ABR component of our model reflects this observation, we convolved the average *Hu* and *Huu* with step functions of different magnitudes (1–5 mmHg). We anticipated that without the *Huu* component, the steady-state ABR response should be linear with respect to the step magnitudes; while by including *Huu* a saturation effect should be observed.

Finally, it has been shown that neck suction when applied during inspiration produces smaller increases in RRI than when applied during expiration.[11] This suggests that there is a respiratory modulation of ABR gain. In order to test the hypothesis that the second-order cross-kernel of our model reflects respiratory modulation of ABR, we performed the following simulation. The average *Hxu* was convolved with a semi-sinusoidal tidal volume pattern (1 L) of 6 s period, and a positive pulsed SBP signal (0.5 s pulse width, magnitude 30 mmHg) triggered at different times along the inspiratory/expiratory cycle. We anticipated that the increase in RRI following each SBP pulse should be different, depending on the timing of the pulse within the respiratory cycle.

RESULTS

Sample Time-Series

A representative segment of data obtained from one of the OSAS subjects is displayed in Fig. 2. A CPAP level of approximately 7 cm H_2O was applied during sleep. The randomly timed increases in inspiratory pressure delivered during the test procedure can be observed in the top panel. The consequent variability imposed on the breathing pattern is quite evident in both tidal volume and breath duration. These respiratory variations, in turn, lead to corresponding fluctuations in SBP and RRI. The occurrence of spontaneous fluctuations in SBP and RRI largely independent of the respiratory changes (e.g., at ~40 s) should be noted.

Summary Statistical Measures

Due to the heavy instrumentation imposed on the subjects, total sleep time was spent primarily in Stage 2 and rapid eye-movement (REM) sleep. Thus, comparisons of the results were made across only three states: wakefulness, REM sleep, and non-REM Stage 2 sleep. The means and standard errors (SE) of the cardiovascular variables in both subject groups are shown in Table 1. RRI was significantly lower in OSAS patients relative to controls ($p < 0.005$), and increased from wakefulness to sleep ($p < 0.02$) in both groups. There was no group or state difference in any of the other summary statistical measures of HRV and blood pressure variability. Average minute ventilation decreased significantly during sleep in both control subjects (awake: 9.0 ± 0.5 L/min, REM: 7.4 ± 0.4 L/min, and Stage 2: 7.2 ± 0.3 L/min) and OSAS patients (awake: 9.9 ± 0.6 L/min, REM: 7.5 ± 0.4 L/min, and Stage 2: 6.8 ± 0.5 L/min), but was not different between groups.

Linear and Nonlinear Model Prediction Accuracy

Model accuracy was evaluated by computing the output prediction normalized mean square error (NMSE). The average NMSE achieved using only the linear (first-order) part of the model was 59.3 ± 3.2% for the control group and 64.5 ± 1.9% for the OSAS group. The average NMSE achieved using the second-order model was 32.2 ± 3.2% for the control group and 34.2 ± 2.4% for the OSAS group. Thus, extending the linear model to include second-order nonlinearities led to a halving of NMSE. This is further illustrated in the frequency domain (Fig. 3): here, the average spectra of the measured RRI signal (solid line) along with the first-order (dotted line) and second-

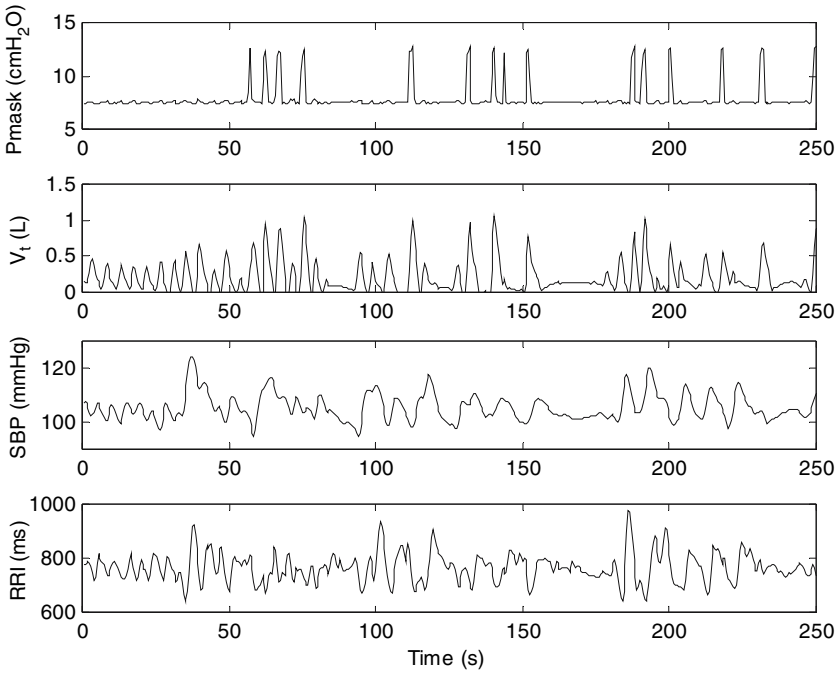

FIGURE 2. Sample trace of the cardiorespiratory signals recorded during a test procedure in an OSAS subject during sleep. The mask pressure tracing (P_{mask}) shows the pulses of +5 cm H_2O randomly introduced by the ventilator, superimposed over a baseline CPAP level of 7 cm H_2O. Corresponding changes in instantaneous lung volume (V_t), systolic blood pressure (SBP), and R–R interval (RRI) are also shown.

TABLE 1. Summary of cardiovascular measures.

	Control			OSA			*p*-Value		
Parameter	Wakefulness	REM	Stage 2	Wakefulness	REM	Stage 2	Group	State	Group × State
Mean RRI (ms)	980 ± 44	1027 ± 39	1045 ± 39	799 ± 39	821 ± 39	812 ± 39	**0.002***	**0.015***	0.194
RRI variability (ms)	49.9 ± 8.3	49.1 ± 7.5	44.4 ± 7.1	44.1 ± 6.6	41.4 ± 5.6	29.3 ± 3.6	0.212	0.098	0.606
Mean SBP (mmHg)	127.1 ± 6.3	122.8 ± 5.7	117.9 ± 4.0	121.1 ± 3.8	125.4 ± 4.3	121.9 ± 3.8	0.970	0.379	0.291
SBP variability (mm Hg)	4.9 ± 0.3	4.1 ± 0.5	4.5 ± 0.3	7.4 ± 1.7	4.7 ± 0.8	4.8 ± 0.5	0.232	0.079	0.384
Mean DBP (mmHg)	69.2 ± 4.6	70.9 ± 4.8	66.6 ± 2.5	65.5 ± 3.2	69.3 ± 2.0	65.7 ± 3.3	0.564	0.405	0.893
DBP variability (mmHg)	3.5 ± 0.7	2.7 ± 0.3	2.8 ± 0.3	5.7 ± 1.4	4.1 ± 0.5	3.4 ± 0.4	0.059	0.108	0.508

RRI: R-R Interval; SBP: Systolic blood pressure; DBP: Diastolic blood pressure.

order (dashed line) model prediction residuals are displayed. The improvement in the output prediction from the first-order to the second-order models is evident by the higher power spectral density of the first-order residuals below 0.3 Hz, and especially below 0.15 Hz. In order to quantify the contribution of the individual second-order dynamics to the model prediction, the NMSE was computed in models that included the linear and each one of the three second-order components at a time. On average, the individual contributions of the second-order kernels were as follows: V_t^2–RRI contribution 7.4 ± 0.7% in controls and 9.4 ± 0.7% in OSAS; SBP^2–RRI contribution 8.8 ± 0.6% in controls and 10.6 ± 0.7% in OSAS; and V_t*SBP–RRI contribution 12.7 ± 0.9% in controls and 15.5 ± 0.9% in OSAS.

Linear Kernels

The impulse responses corresponding to the two mechanisms are consistent with the underlying physiology. Representative RCC impulse responses from the control and OSAS groups are shown in Fig. 4 (left panels). The RCC linear kernel, representing the linear dynamics of the central component of the respiratory sinus arrhythmia, shows a fast negative peak (increase in heart rate during inspiration) and a lead (negative delay) between the HR and the V_t. Representative ABR impulse responses are also displayed in Fig. 4 (right panels). The ABR impulse response increases initially to positive values, reflecting a very rapid decrease in HR (increase in RRI) in response to an increase in ABP. The magnitudes of the impulse

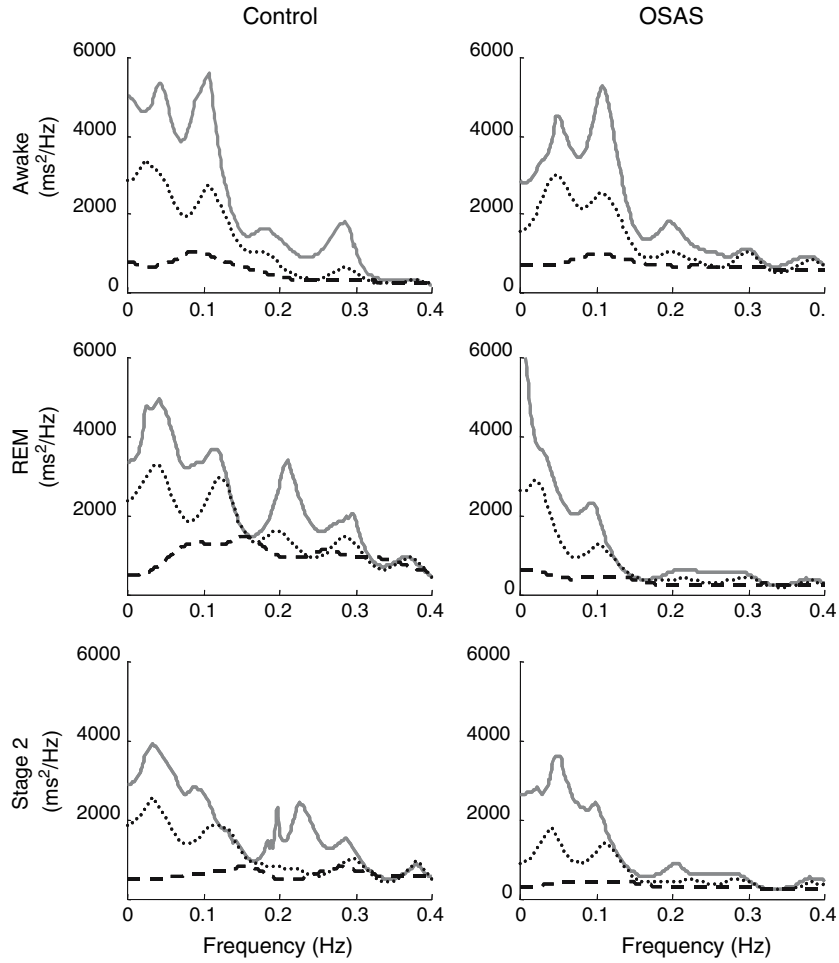

FIGURE 3. Average spectra of the RRI signal (solid lines) and the first-order (dotted lines) and second-order (dashed lines) residuals, for the control and OSAS groups, during wakefulness, REM and Stage 2 sleep. Second-order residuals are considerably lower with respect to the first-order residuals at frequencies below 0.15 Hz, and especially below 0.08 Hz.

responses corresponding to the control subject were larger than the ones from the OSAS subject for both RCC and ABR mechanisms, except for ABR during wakefulness.

Second-Order Kernels

Representative V_t^2–RRI second-order kernels are shown in Fig. 5. The V_t^2–RRI kernels presented distinct shapes and very slow dynamics (lasting longer than the 40 s), indicating the presence of complex and very slow frequency contributions. The kernel amplitudes were larger during sleep relative to wakefulness, especially in the control subject. Sample SBP^2–RRI second-order kernels are shown in Fig. 6. Although the SBP^2–RRI kernels also presented distinct shapes, they were less irregular than those for the V_t^2–RRI kernels. Moreover, the SBP^2–RRI kernels presented a fast large peak within the first 10 s and decayed within 40 s, reflecting relatively faster dynamics. The kernel amplitudes from the control subject were larger than those from the OSAS patient, during both wakefulness and sleep. Sample V_t*SBP–RRI second-order kernels are also shown in Fig. 7. These kernels presented a combination of both slow and fast dynamics, aligned to the V_t and SBP axes respectively, which is consistent with the type of time responses found in the self-kernels described before.

Statistical Comparison of Model Parameters

Table 2 displays the group-averaged results (mean ± SE) for all compact descriptors derived from the RCC and ABR impulse responses. The linear RCC gain index (IRM_{RCC}) was smaller in the OSAS subjects relative to controls ($p < 0.04$). In both subject groups, there was little change in IRM_{RCC} across sleep–wake states (Fig. 8, top-left panel). Latency of the RCC

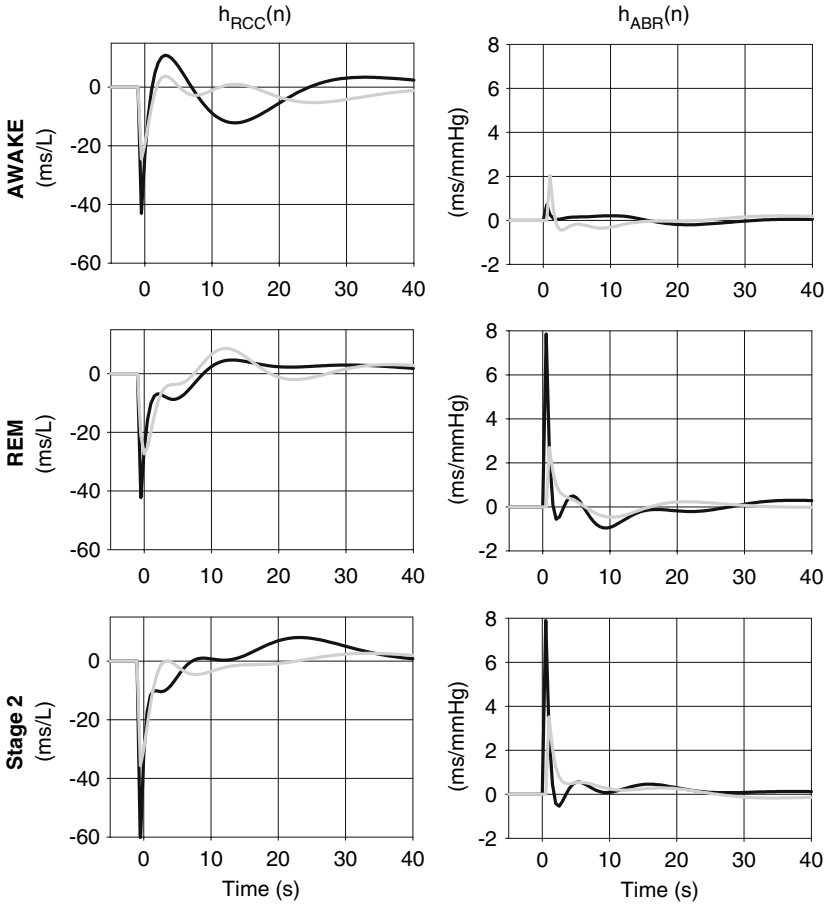

FIGURE 4. Representative tracings of the RCC and ABR model impulse responses estimated from a normal control (dark tracings) and OSAS patient (light tracings) during wakefulness, REM, and Stage 2 sleep. The impulse response amplitudes corresponding to the control subject were larger than the ones from the OSAS subject for both RCC and ABR mechanisms, except for ABR during wakefulness.

impulse responses was more negative in the OSAS patients relative to controls ($p < 0.04$), but unchanged with sleep–wake state.

The ABR gain (IRM_{ABR}) was lower in the OSAS subjects relative to controls ($p < 0.04$) and increased almost significantly from wakefulness to sleep; however, this increase was clearly much greater in the controls (IRM_{ABR} was approximately twice as large in sleep relative to wakefulness in the control subjects, while it was no significant dependence of the ABR gain on state in the OSAS patients; Fig. 8, top-right panel).

Table 2 also displays the group-averaged results (mean ± SE) for all compact descriptors derived from the second-order self- and cross-kernels. The V_t^2–RRI gain ($KM_{V_t^2}$) increased from wakefulness to sleep in both control subjects and OSAS patients ($p < 0.03$). The SBP^2–RRI gain (KM_{SBP^2}) was higher in controls vs. OSAS patients ($p < 0.0001$). KM_{SBP^2} also increased almost twice from wakefulness to Stage 2 sleep in the controls, while there was no significant dependence of the SBP^2–RRI gain on state in the OSAS patients (Fig. 8, bottom-left panel). The V_t*SBP–RRI gain ($KM_{V_t{}^*SBP}$) was higher in controls relative to OSAS patients ($p < 0.002$), but did not change significantly across wake–sleep states (Fig. 8, bottom-right panel).

Simulation Results for Physiological Interpretation of Nonlinear Kernels

The normalized frequency response of the linear and nonlinear RCC components to a chirp V_t signal of different levels is shown in Fig. 9. For both Control and OSAS groups, the linear RCC responses were independent of tidal volume. In contrast, the combined linear/nonlinear RCC response was affected by tidal volume in both groups. As tidal volume increased from 0.5 to 3 L, the nonlinear RCC responses also increased, particular at frequencies below 0.3 Hz. Both the linear and nonlinear RCC responses were larger in the Control group compared to the OSAS group. The increase in the nonlinear RCC response with tidal

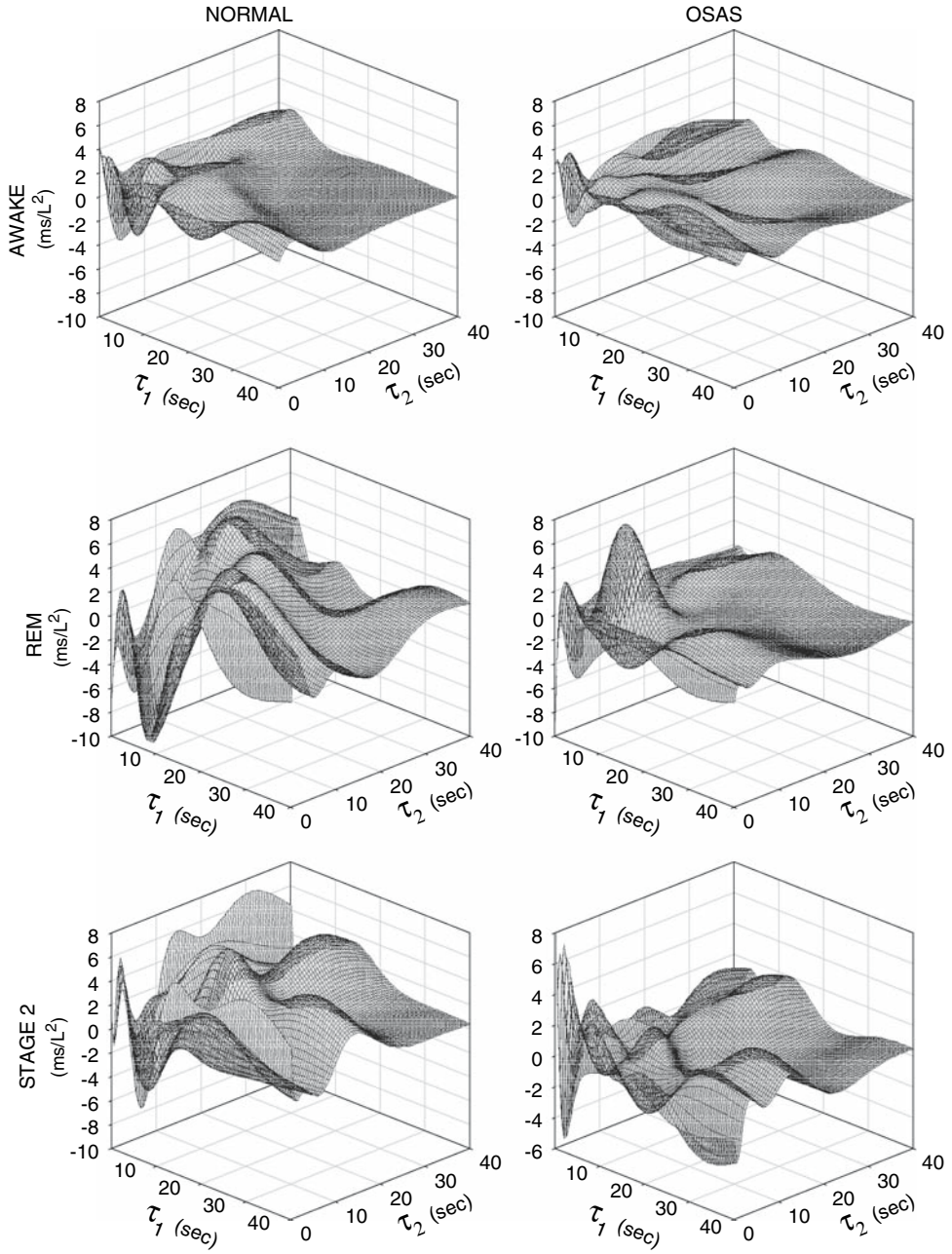

FIGURE 5. Representative V_t^2–RRI second-order kernels, corresponding to wakefulness, REM, and Stage 2 sleep in the control and OSAS subjects shown in Fig. 4. Note that kernel amplitudes were higher in sleep vs. wakefulness in both subjects.

volume level was more pronounced in the OSAS than in the Control group.

The step-responses for the linear and nonlinear components of ABR for different SBP step magnitudes are shown in Fig. 10. A steady-state level was achieved within 30 s in both groups. The linear ABR step-responses increased as the SBP step magnitude increased, as expected. The nonlinear ABR step-responses, on the other hand, were negative and decreased as the SBP step magnitude increased. The resulting combined linear and nonlinear ABR step-responses also increased with the SBP step magnitude, although as the step became larger, the differential increase became smaller. This can be better visualized in the bottom panels, which display the steady-state values achieved under the different step magnitudes tested. The first-order steady-state ABR responses were linearly related to the SBP step-size, while the combined first/second-order steady-state ABR responses increased less rapidly with the respect to the step magnitude,

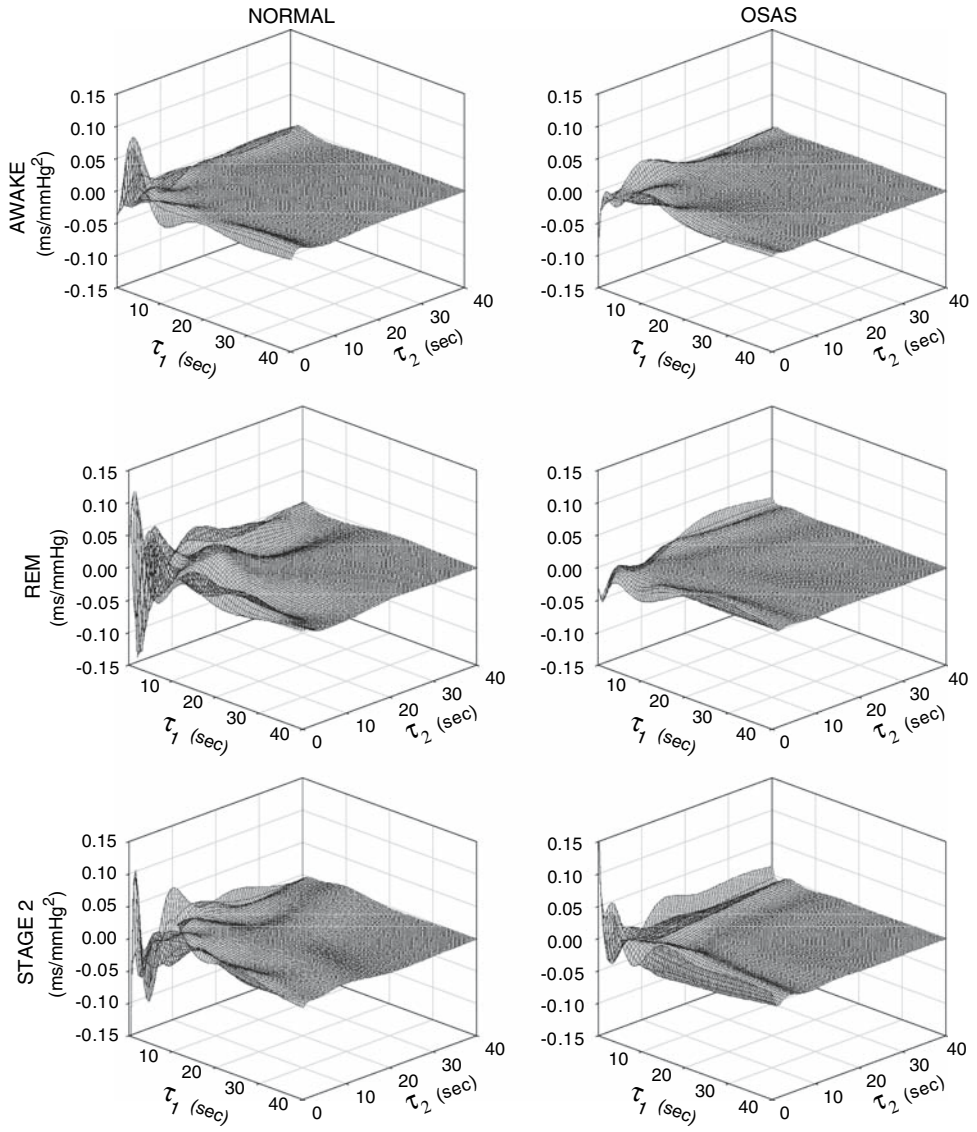

FIGURE 6. Representative SBP^2–RRI second-order kernels, corresponding to wakefulness, REM, and Stage 2 sleep in the same control and OSAS subjects displayed in Fig. 4. Kernel amplitudes were larger in the control relative to the OSAS subject, but there appears to be little dependence on state.

demonstrating a tendency to saturate with increasing step magnitude.

Figure 11 shows the results of model simulations in which the linear and nonlinear baroreflex components were stimulated by BP pulses at different times during the respiratory cycle. In both types of subjects, the ABR pulse response was larger when the SBP pulse was triggered during expiration than during inspiration. In the control group, the ABR pulse response decreased to ~80% of its mean value (~50 ms) at mid inspiration, and started to increase to ~120% of its mean values at mid expiration. This behavior is similar to the experimental results obtained by Eckberg[11] using neck suction to stimulate the baroreceptors. In the OSAS group, the decrease in ABR pulse response during inspiration was minimal, but the increase during expiration was more substantial. As expected, the ABR pulse responses in OSAS were smaller in overall level than those in the controls because of the reduced linear and nonlinear baroreflex gains in the former group.

DISCUSSION

Delineation of Major Components of HRV

HRV is modulated primarily from neural and mechanical coupling of the respiratory and cardiovascular systems, lung vagal, and baroreflex

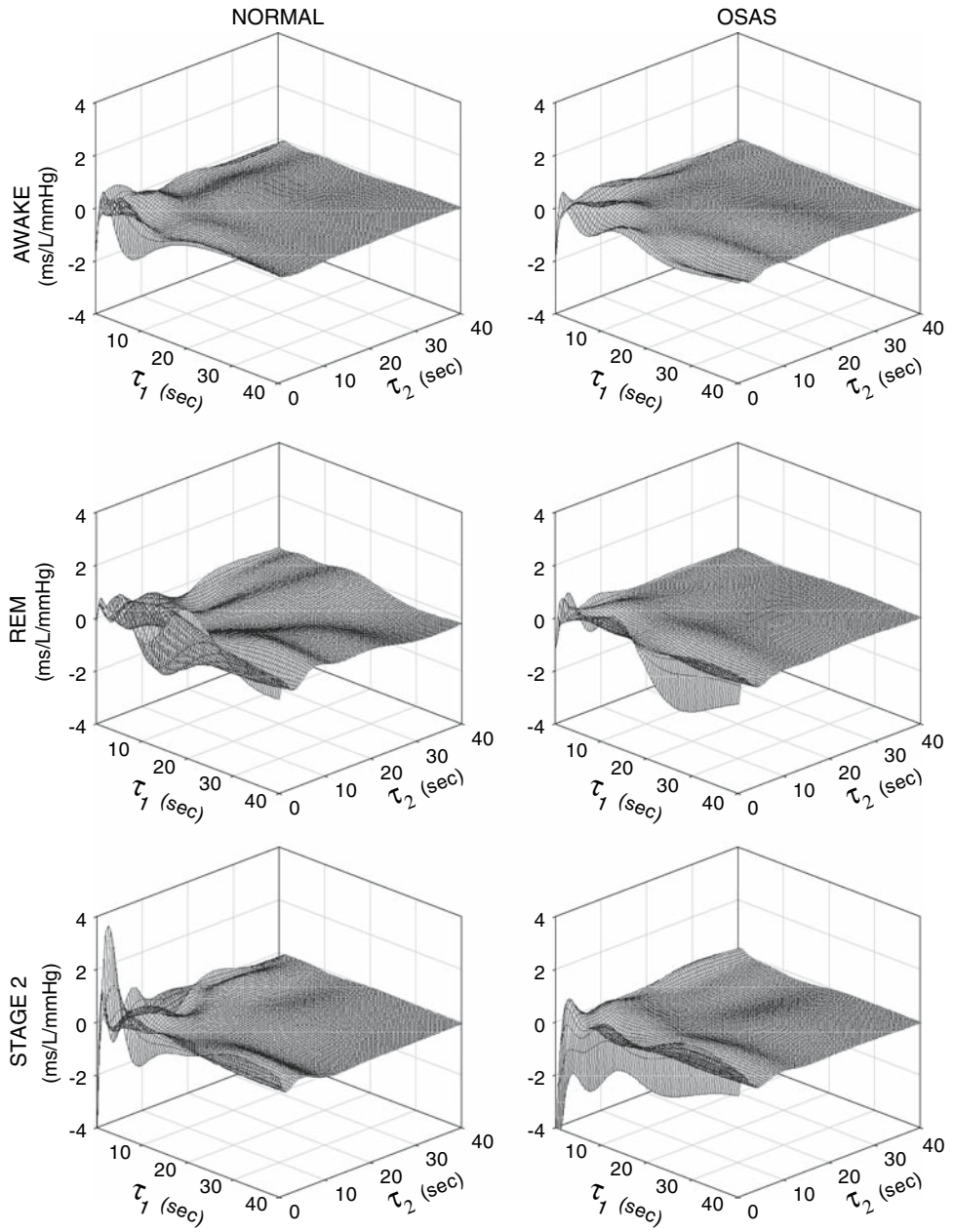

FIGURE 7. Sample V_t*SBP–RRI second-order cross-kernels, corresponding to wakefulness, REM, and Stage 2 sleep in the same control and OSAS subjects displayed in Fig. 4. See text for further details.

feedbacks.[10] Central to the method introduced in this study is the mathematical model that allows delineation of these respiratory and baroreflex contributions. Although respiration and blood pressure are treated as mutually independent inputs, together with heart rate, are part of a larger closed-loop control system.[1,17] By imposing physiological delays in this closed-loop system, feedforward and feedback dynamics can be separated, in essence, allowing the loop to be "computationally opened."[20] For instance, in the baroreflex portion of the closed-loop system, present changes in RRI are constrained to be influenced only by past fluctuations of blood pressure. This imposed constraint (termed "causality" in systems engineering terminology) forces the estimation scheme to converge towards a solution that reflects the effect of blood pressure on RRI (i.e., the baroreflex), rather than the effects of RRI on blood pressure (i.e., the feedforward component). This "temporal delineation" approach can only be formulated in the time domain and has been extensively used in cardiovascular control system identification.[1,8,17,29] In contrast, frequency-domain

TABLE 2. Linear and nonlinear gain estimates.

	Control			OSA			*p*-Value		
Parameter	Wake	REM	Stage 2	Wake	REM	Stage 2	Group	State	Group × State
Linear parameters									
RCC IR magnitude (ms/L)	47.8 ± 8.5	51.0 ± 7.7	53.6 ± 8.5	25.5 ± 5.1	33.8 ± 5.5	28.4 ± 6.5	**0.037**	0.054	0.246
ABR IR magnitude (ms/mmHg)	2.21 ± 0.44	4.34 ± 0.92	3.71 ± 0.77	1.84 ± 0.42	1.75 ± 0.34	2.19 ± 0.42	**0.032**	0.053	0.058
Nonlinear parameters									
V_t^2–RRI kernel magnitude (ms/L^2)	25.8 ± 4.7	34.7 ± 8.6	37.2 ± 5.4	14.8 ± 2.7	28.4 ± 4.6	24.3 ± 6.5	0.128	**0.025**	0.737
SBP^2–RRI kernel magnitude ($ms/mmHg^2$)	0.19 ± 0.07	0.24 ± 0.04	0.38 ± 0.08	0.07 ± 0.02	0.09 ± 0.01	0.06 ± 0.01	<**0.0001**	0.174	0.085
V_t*SBP–RRI kernel magnitude ($ms/L^1/mmHg^2$)	4.32 ± 0.91	5.12 ± 0.58	5.48 ± 0.69	1.98 ± 0.35	3.21 ± 0.62	2.64 ± 0.30	**0.002**	0.084	0.62

RCC: respiratory–cardiac coupling component; ABR: arterial baroreflex component.

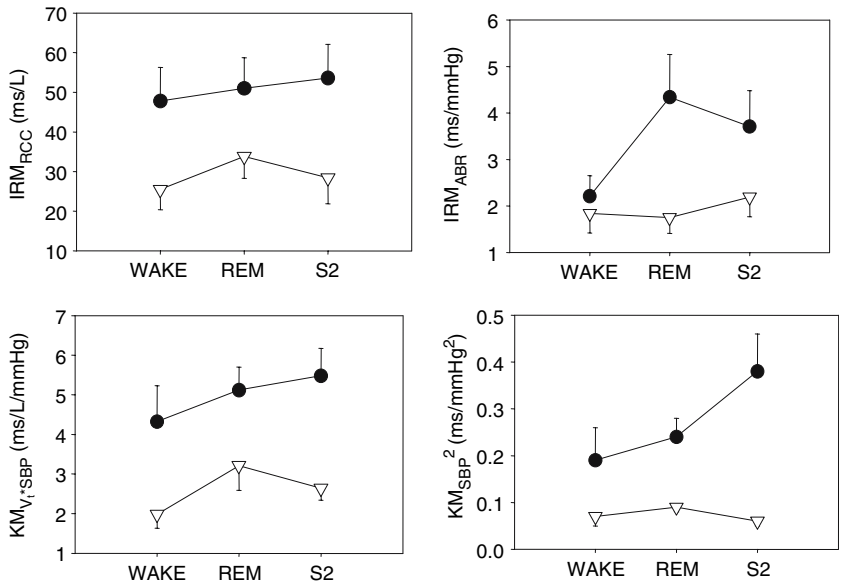

FIGURE 8. Average values of the linear and nonlinear gains for the control (filled circles) and OSAS (open triangles) groups are presented here. RSA gain (IRM_{RSA}) was significantly higher in controls vs. OSAS, but was unchanged with sleep–wake state. Baroreflex gain (IRM_{ABR}) was also higher in controls vs. OSAS patients, and increased substantially in controls, while was only slightly elevated in the OSAS. SBP^2–RRI gain (KM_{SBP^2}) was higher in controls vs. OSAS, especially during Stage 2 sleep. V_t*SBP–RRI gain (KM_{V_t*SBP}) was higher in controls vs. OSAS.

methods (i.e., cross-spectral analysis) do not allow the implementation of causality constraints.

In principle, the estimation of the linear and nonlinear kernels of our model is best achieved when the corresponding inputs, SBP and V_t, are independent of each other.[8] Changes in intrathoracic pressure during respiration, however, can induce changes in blood pressure. Fortuitously, other influences, such as variations in cardiac output and peripheral resistance, also contribute to spontaneous fluctuations in SBP. In our study, application of the test protocol helped to further decorrelate V_t and SBP, since on any given breath, inspiration can result in either a decrease or increase in SBP. Which way SBP is affected depends on the relative amounts of active breathing vs. assistance provided by the ventilator during that breath.[17]

Nonlinear Contributions of V_t and SBP to HRV

The nonlinear characteristics involved in the modulation of HRV were confirmed by comparing the prediction NMSE achieved by the linear and nonlinear models. The prediction NMSE was reduced by ~30% when second-order terms were included in the model, showing that second-order dynamics cannot be neglected. It was also observed that the individual con-

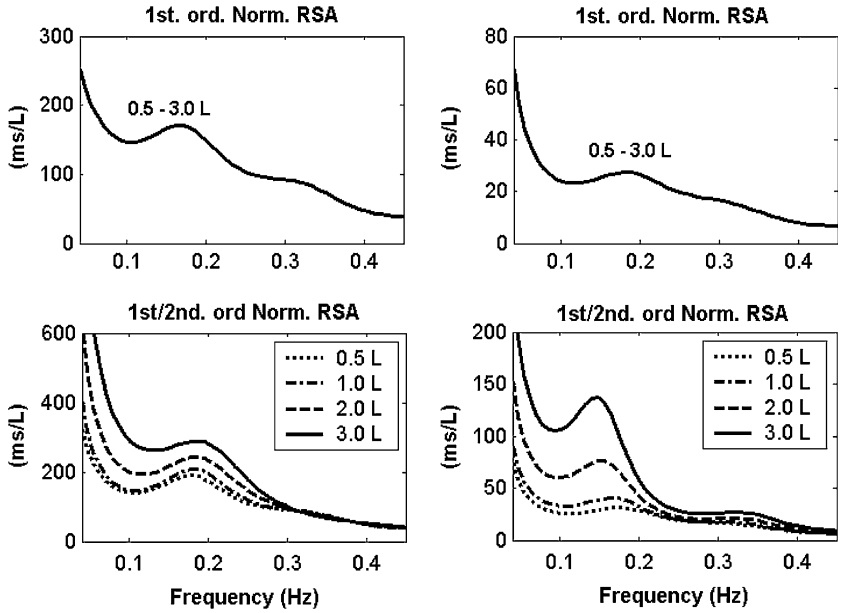

FIGURE 9. Normalized frequency responses of the linear (top) and combined linear + nonlinear (bottom) RSA components for the Control (left) and OSAS (right) groups, for different values of tidal volume. Note that the ordinate scales for the frequency responses in the Control group (left panel) are substantially larger than the corresponding scales for the OSAS group (right panel).

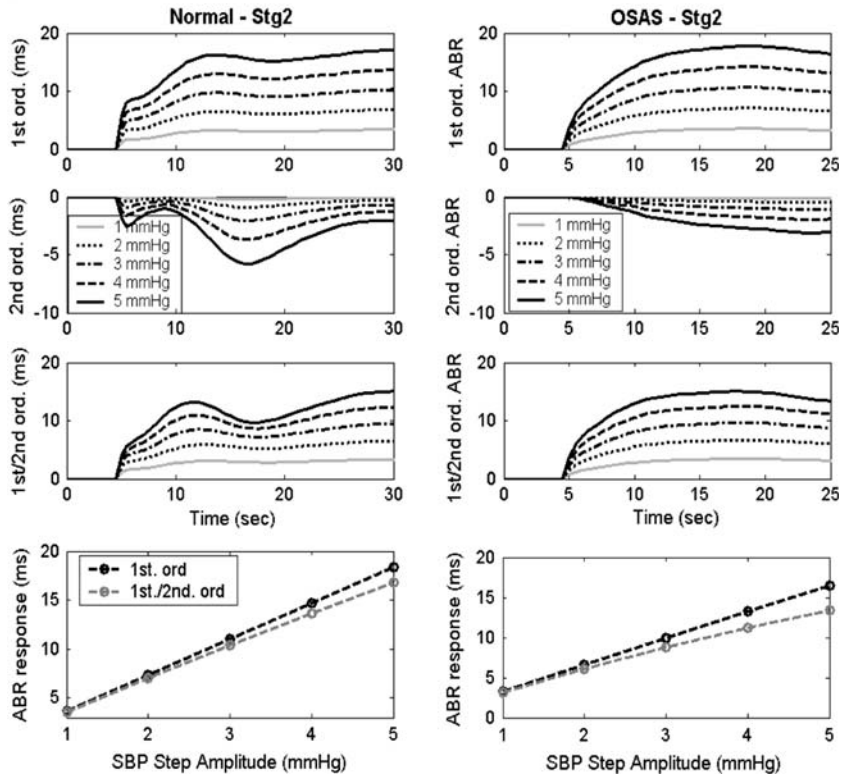

FIGURE 10. Linear (top panels), nonlinear (second row), and overall (third row) ABR step-responses to a SBP step input of different amplitudes (1–5 mmHg), for the Control (left) and OSAS (right) groups. The bottom panels each display the overall ABR steady-state response as a function of SBP step magnitudes.

tribution of the second-order kernels were higher for the SBP^2–RRI and V_t*SBP–RRI components, indicating that nonlinear mechanisms involving SBP interactions, contribute more to HRV.

Analysis of the spectral content of the first- and second-order model residuals (output prediction error) demonstrated that the second-order nonlinearities make a significant contribution to the RRI

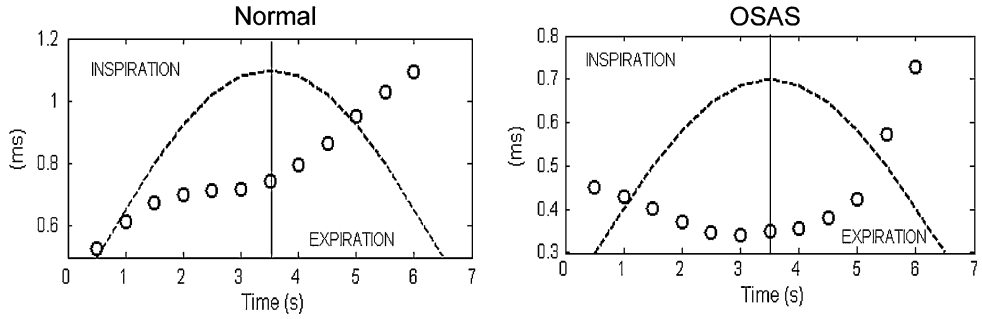

FIGURE 11. Peak responses of the RCC-ABR cross-kernel to a 30 mmHg SBP pulse train triggered at different times during the inspiratory/expiratory cycle, simulating the neck suction experiments of Eckberg and Orshan.[11] In both subject groups, baroreflex stimulation exerted a greater effect during expiration than in inspiration. Top panel: Normal control; Bottom panel: OSAS subject.

spectrum at the low and very low frequency range (below 0.15 Hz and mostly below 0.08 Hz). This finding is consistent with a number of previous studies. Mullen *et al.*,[29] when studying the effects of posture and autonomic blockade on a cardiovascular closed-loop linear model of similar structure, observed that the power of the residuals of the HRV model were concentrated at frequencies below 0.1 Hz; they attributed these effects to the presence of nonlinear coupling mechanisms. A similar concentration of the residual power at frequencies below 0.1 Hz was found by Mukkamala *et al.*,[28] when they applied a similar linear model of HRV to assess impairment of autonomic control in patients with diabetic autonomic neuropathy. Chon *et al.*[8] demonstrated that the residuals of the linear portion of their model, concentrated at frequencies below 0.08 Hz, were reduced significantly after they included second-order nonlinear components to the model. Consistent with these previous studies, our results have also shown a concentration of the first-order residuals at frequencies below 0.08 Hz that are largely eliminated in the nonlinear model. Moreover, we have determined from careful analysis of the contributions of the inputs and their cross-correlations with the residuals that the very low-frequency residual power may be attributed mostly to nonlinearity in the baroreflex contribution and the effect of nonlinear ABP–V_t interaction on HRV.

Linear Dynamics

The impulse responses (first-order kernels) corresponding to the two mechanisms are consistent with the underlying physiology, similar to the results from the 2-input linear model of HRV presented in our previous studies.[1,17] The RCC impulse response, which represents the mainly vagal coupling between respiration and heart period, shows a fast initial negative peak and a lead (negative delay) between the HR and V_t, reflecting an increase in heart rate during inspiratory effort, starting before the onset of the actual mechanical inspiration. The baroreflex impulse response increases initially to positive values, reflecting a very rapid decrease in HR (increase in RR interval) in response to an increase in ABP.

The RCC gain index extracted from the impulse responses was statistically higher in controls vs. OSAS in all states, indicating that the mainly parasympathetically mediated RCC mechanism is suppressed in these patients during both wakefulness and sleep. In addition, the fact that the RCC impulse response starts earlier but its peak occurs later in the OSAS patients suggests that the RCC mechanism is not only depressed in this group, but requires a longer time to fully modulate heart rate. The increase on the average ABR impulse response magnitudes from wakefulness to sleep in the control group supports the notion that baroreflex gain increases during sleep.[25] The fact that the average ABR impulse responses were smaller in magnitude in the OSAS and did not change across wake–sleep states, indicates an impaired baroreflex control in these patients. Results from the statistical analysis of the ABR gain fully support the previous findings. Overall, the results on the first-order kernels of the two main mechanisms RCC and ABR identified using the second-order model of HRV are in excellent agreement with our results from the linear model reported in the previous study.[17] One advantage in using the nonlinear model, however, is that it provides better model prediction and probably better parameter estimation.

Second-Order Dynamics

The distinct shapes and tendency for the V_t^2–RRI second-order self-kernels to decay over relatively long periods of time indicate the presence of very complex and mainly slow dynamics involved in the nonlinear effects of respiration on heart rate. As well, the

significant increase in the magnitudes of the V_t^2–RRI kernels from wakefulness to sleep in both the control and OSAS suggests that the nonlinear effects of respiration on heart rate play a more important role during sleep. All the linear indexes of RCC gain presented here and in our previous study[17] represent direct respiratory modulation of heart rate, mainly via parasympathetic activity, since the mechanisms represented by these indices work at frequencies above 0.1 Hz, where the sympathetic system is unable to modulate heart rate. On the other hand, the nonlinear component of RCC gain (V_t^2–RRI interaction), which contains very low frequency dynamics, may be mediated by both sympathetic and parasympathetic activity, as was shown in the study by Chon *et al.*[8] In their study, it was observed that following propanolol administration (sympathetic blockade), the V_t^2–RRI kernel amplitudes became smaller, but the decrease was more evident after atropine administration (parasympathetic blockade). Thus, the fact that V_t^2–RRI kernel magnitudes increased during sleep suggests that both sympathetically and parasympathetically mediated nonlinear effects of respiration in the modulation of heart rate are increased during sleep. In contrast to the linear RCC gains, the V_t^2–RRI kernel magnitudes were similar in the control and OSAS groups, indicating that only the linear component of RCC is altered in OSAS.

Mechanisms involved in the SBP^2–RRI interaction appear to present less complex but much faster dynamics than those observed in V_t^2–RRI interaction. In the study of Chon *et al.*,[8] the amplitude of the SBP^2–RRI decreased considerably after the application of double autonomic blocking agents (propanolol and atropine). However, when only either propanolol (sympathetic blockade) or atropine (parasympathetic blockade) was applied, only a modest reduction in the SBP^2–RRI was observed. These results indicate that both vagal and sympathetic modulations are involved in the nonlinear interactions between blood pressure and heart rate, but in the absence of one of these two factors, the remaining factor is still able to significantly mediate the nonlinear interaction between blood pressure and heart rate. Therefore, our results, which show a dramatic significant decrease in the magnitudes of the SBP^2–RRI kernels from the OSAS group relative to those from the control group (notice the achieved $p < 0.0001$), strongly support the notion that both sympathetic and parasympathetic functions involved in the nonlinear arterial baroreflex modulation of heart rater are impaired in OSAS patients. It is also interesting to observe that the SBP^2–RRI kernel magnitude increased from wakefulness to sleep (almost two-fold during Stage 2 sleep) in the control group, while it was almost unchanged in the OSAS group. These findings and the results from the linear ABR gains indicate that both the linear and nonlinear components of the arterial baroreflex mechanism increased during sleep under normal conditions, while in OSAS patients both linear and nonlinear dynamics of ABR are diminished.

Chon *et al.*[8] also reported a reduction in V_t*SBP–RRI kernel magnitude after either atropine or propanolol administration, indicating that the contribution to HRV from the interaction between ABP and respiration is mediated by both vagal and sympathetic pathways. Our estimates of the V_t*SBP–RRI kernel show that the interactions between fast changes in SBP and fast and slow changes in V_t are attenuated in the OSAS subjects, further suggesting impairment of both sympathetic and parasympathetic control in these patients.

One of the disadvantages of employing the Volterra approach to model nonlinear dynamics is that the complexity of the model grows very rapidly as the order of the dynamics increases. Kernels that are third-order or higher are difficult even to represent on a graphical basis, since three-dimensional plots of the kernel yield information of only a "slice" through one of the dimensions. Thus, truncating the model to second order is somewhat arbitrary and could lead to the omission of potentially important nonlinear dynamics. On the other hand, our tests of the residuals following the application of the second-order model showed that these were largely broad-band (see Fig. 3), suggesting that much of the dynamics was indeed captured by the model. Our findings are supported by a previous study by Chon *et al.*,[8] who similarly employed a second-order Volterra model to investigate HRV. An alternative approach has been to use "block-structured" models that contain interconnections of dynamic linear systems and static nonlinearities.[36] These types of models allow some highly nonlinear systems to be characterized with a relatively small number of parameters. The drawback here is that an incorrect assumption of the system structure would also lead to incorrect model identification. There are a number of simple cases in which one-to-one correspondences between Volterra kernel models and block-structured models can be easily identified. For instance, if the actual underlying system could be described as a "Hammerstein" model, consisting of a static nonlinearity followed by a linear dynamic system, the second-order kernel would be zero everywhere except along the diagonal ($\tau_1 = \tau_2$). In the case of a "Wiener" model, consisting of a linear dynamic system followed by a static nonlinearity, any "slice" of the second-order kernel at fixed τ_2 would be proportional to the first-order kernel. We examined our estimated second-order kernels for these special features but did not find them.

Physiological Interpretation of Current Findings

As mentioned earlier, the complexity of second- and higher-order Volterra kernels greatly complicate our ability to interpret the physiological ramifications of these models. To alleviate this problem, we performed simulations with the estimated models that mimicked physiological experiments. Simulations of the RSA response derived from our linear and nonlinear kernels confirmed a dependency of the RSA frequency response upon the tidal volume.[10,15] More interestingly, this tidal volume dependency increases with increasing magnitude of the nonlinear (second-order) dynamics between respiration and heart rate fluctuations. Simulations of the ABR steady-state response derived from our linear and nonlinear kernels confirmed a saturation in the SBP–RRI relation. The simulations also demonstrate that the rapidity with which the increases in RRI saturate as SBP is increased depends on the magnitude and form of the second-order kernel relating blood pressure to RRI fluctuations.

Simulations of the RSA–ABR nonlinear interaction derived from our second-order cross-kernel indicate a respiratory modulation of baroreflex gain. For both controls and OSAS, the ABR response was larger during expiration than during inspiration, as had been previously observed by Eckberg and Orshan.[11] This results provide additional evidence of the existence of an interaction between respiratory and baroreceptor reflexes, and suggest that the quality of the central autonomic modulation depends upon the level of afferent baroreceptor activity and the depth of inspiration.[10] It is important to note, however, that this effect is small relative to the combined effects of all other components of our model.

How does OSAS lead to detrimental consequences for the autonomic regulation of the cardiovascular system? Although the pathophysiological pathways remain unresolved, a number of important animal studies[5,12] suggest that chronic exposure to episodic hypoxia, which stimulates the peripheral chemoreflexes acutely, leads to a resetting of chemoreceptor function. This, in turn, suppresses baroreceptor function, leading to a sustained increase in sympathetic tone.[13] It is also possible that the concomitant exposure to episodic arousal from sleep, which generally accompanies the termination of obstructive apnea, could play a contributory role in the genesis of sympathetic overactivity.[4]

Potential Confounding Effects of CPAP

In the OSAS patients, CPAP at their individually prescribed levels was applied during sleep in order to ensure upper airway patency throughout the test procedure. This was an important part of the experimental procedure, since it enabled us to assess autonomic control across different sleep–wake states and across individuals under relatively similar patterns of respiration and under stable stages of sleep. In contrast, previous investigations of autonomic control in OSAS during sleep were carried out under uncontrolled conditions in which the episodes of obstructive apnea were associated with profound swings in sympathetic and parasympathetic activity as well as transient state changes.[19,35] The occurrence of large swings in respiration and the cardiovascular variables can lead to severe distortions of the HRV and blood pressure variability spectra, and thus contribute to interpretational difficulties if these spectral measures are used for making inferences about autonomic function.[21]

On the other hand, CPAP application in the OSAS patients during sleep may have led inevitably to some confounding influences. For example, in subjects with normal heart function, acute application of CPAP is known to decrease left ventricular preload more than left ventricular afterload, leading to a reduction in cardiac output.[9] However, our OSAS subjects did not show any change in SBP or DBP during sleep relative to wakefulness when only minimal CPAP was applied. The CPAP-induced increase in lung volume itself may have also contributed to some increase in vagal activity and reduction in sympathetic drive.[6] Therefore, our technique is likely to have *underestimated* the extent of autonomic abnormality in the OSAS subjects during sleep.[17]

CONCLUSIONS

In this study, we have applied a second-order model to determine the presence of nonlinear interactions in the regulation of HRV, as well as to investigate how these interactions are affected by OSAS and by different wake–sleep states. Our results showed a significant nonlinear component of HRV, concentrated primarily at frequencies below 0.08 Hz, confirming previous results. Second-order interactions related to the baroreflex constituted the most significant nonlinear component involved in HRV. It was also demonstrated that both linear and nonlinear dynamics involved in the regulation of HRV are altered in OSAS and depend to some extent on sleep–wake state. Finally, this study provides simple physiological interpretations to the second-order dynamics derived by our nonlinear model of HRV. The second-order kernels reflect specific characteristics of the RCC and ABR mechanisms, such as dependence of RCC on tidal volume, saturation in the SBP–RRI relation, and respiratory modulation of baroreflex gain. In

summary, the application of the nonlinear model-based approach to quantify linear and nonlinear dynamics involved in the autonomic control of heart rate constitutes a useful, insightful and comprehensive approach for the detection and assessment of abnormal autonomic function in OSAS during wakefulness and sleep. This noninvasive method could also be useful for evaluating autonomic dysfunction in other disease conditions, such as diabetes, Parkinson disease and Shy–Drager syndrome.

REFERENCES

[1]Belozeroff, V., R. B. Berry, C. S. H. Sassoon, and M. C. K. Khoo. Effects of CPAP therapy on cardiovascular variability in obstructive sleep apnea: a closed-loop analysis. *Am. J. Physiol.: Heart Circ. Physiol.* 282:H110–H121, 2002.

[2]Berger, R. D., S. Akselrod, D. Gordon, and R. J. Cohen. An efficient algorithm for spectral analysis of heart rate variability. *IEEE Trans. Biomed. Eng.* 33:900–904, 1986.

[3]Blasi, A., J. Jo, E. Valladares, E. Juarez, A. Baydur, and M. C. K. Khoo. Autonomic cardiovascular control following transient arousal from sleep: a time-varying closed-loop model. *IEEE Trans. Biomed. Eng.* 53:74–82, 2006.

[4]Blasi, A., B. J. Morgan, J. B. Skatrud, J. Jo, E. Valladares, and M. C. K. Khoo. Autonomic cardiovascular control following arousal from sleep: time-varying spectral analysis. *J. Appl. Physiol.* 95:1394–1404, 2003.

[5]Brooks, D., R. L. Horner, L. F. Kozar, C. L. Render-Texeira, and E. A. Phillipson. Obstructive sleep apnea as a cause of systemic hypertension: evidence from a canine model. *J. Clin. Invest.* 99:106–109, 1997.

[6]Butler, G. C., M. T. Naughton, M. A. Rahman, T. D. Bradley, and J. S. Floras. Continuous positive airway pressure increases heart rate variability in congestive heart failure. *J. Am. Coll. Cardiol.* 25:672–679, 1995.

[7]Chon, K. I., Y. M. Chen, V. Z. Marmarelis, D. J. Marsh, and N. H. Holstein-Rathlou. Detection of interactions between myogenic and TGF mechanisms using nonlinear analysis. *Am. J. Physiol.* 36:F160–F173, 1994.

[8]Chon, K., T. J. Mullen, and R. J. Cohen. A dual-input nonlinear system analysis of autonomic modulation of heart rate. *IEEE Trans. Biomed. Eng.* 43:530–544, 1996.

[9]De Hoyos, A., P. P. Liu, D. C. Benard, and T. D. Bradley. Hemodynamic effects of continuous positive airway pressure in humans with normal and impaired left ventricular function. *Clin. Sci. (Colch)* 88:173–178, 1995.

[10]Eckberg, D.Respiratory sinus arrhythmia and other human cardiovascular neural periodicities. In: Regulation of Breathing, edited by J. A. Dempsey and A. I. Pack. (2nd ed.New York: Dekker, 1995, pp. 669–740.

[11]Eckberg, D. L., and C. R. Orshan. Respiratory and baroreceptor reflex interactions in man. *J. Clin. Invest.* 59:780–785, 1977.

[12]Fletcher, E. C., J. Lesske, R. Behm, C. C. Miller, and T. Unger. Carotid chemoreceptors, systemic blood pressure, and chronic episodic hypoxia mimicking sleep apnea. *J. Appl. Physiol.* 72:1978–1984, 1992.

[13]Francis, D. P., A. J. S. Coats, and P. Ponikowski.Chemoreflex-baroreflex interactions in cardiovascular disease. In: Sleep Apnea: Implications in Cardiovascular and Cerebrovascular Disease, edited by T. D. Bradley and J. S. Floras. New York: Marcel Dekker, 2000, pp. 33–60.

[14]Goldberger, J. J., S. Challapalli, T. Tung, M. A. Parker, and A. H. Kadish. Relationship of heart rate variability to parasympathetic effect. *Circulation* 103:1977–1983, 2001.

[15]Hirsch, J. A., and B. Bishop. Respiratory sinus arrhythmia in humans: how breathing pattern modulates heart rate. *Am. J. Physiol.* 241:H620–H629, 1981.

[16]Huikuri, H. V., T. H. Makikallio, C. K. Peng, A. L. Goldberger, U. Hintze, and M. Moller. Fractal correlation properties of R-R interval dynamics and mortality in patients with depressed left ventricular function after an acute myocardial infarction. *Circulation* 101:47–54, 2000.

[17]Jo, J. A., A. Blasi, E. Valladares, R. Juarez, A. Baydur, and M. C. K. Khoo. Model-based assessment of autonomic control in obstructive sleep apnea syndrome during sleep. *Am. J. Respir. Crit. Care Med.* 167:128–136, 2003.

[18]Jo, J. A., A. Blasi, E. Valladares, R. Juarez, A. Baydur, and M. C. K. Khoo. Determinants of heart-rate variability in Obstructive Sleep Apnea Syndrome during wakefulness and sleep. *Am. J. Physiol. (Heart Circ. Physiol.)* 288:H1103–H1112, 2005.

[19]Keyl, C., P. Lemberger, M. Dambacher, P. Geisler, K. Hochmuth, and A. W. Frey. Heart rate variability in patients with obstructive sleep apnea. *Clin. Sci.* 91(Suppl):56–57, 1996.

[20]Khoo, M. C. K. Physiological Control Systems: Analysis, Simulation and Estimation. Wiley/IEEE Press, 2000.

[21]Khoo, M. C. K., T. S. Kim, and R. B. Berry. Spectral indices of cardiac autonomic function in obstructive sleep apnea. *Sleep* 22:443–451, 1999.

[22]Lee, Y., and M. Schetzen. Measurement of the Wiener kernels of a nonlinear system by cross-correlation. *Int. J. Control* 2:237–254, 1965.

[23]Levy, M. N. Sympathetic-parasympathetic interactions in heart. *Circ. Res.* 29:437–445, 1971.

[24]Makikallio, T. H., J. M. Tapanainen, M. P. Tulppo, and H. V. Huikuri. Clinical applicability of heart rate variability by methods based on nonlinear dynamics. *Cardiac Electrophysiol. Rev.* 6:250–255, 2002.

[25]Mancia, G. and A. L. Mark. Arterial baroreflexes in humans. In: Handbook of Physiology. The Cardiovascular System. Peripheral Circulation and Organ Blood Flow, sect. 3, vol. III, pt. 2, Chapt. 20. Bethesda, MD: Am. Physiol. Soc., 1983, pp. 755–793.

[26]Marmarelis, V. Z. Identification of nonlinear biological systems using Laguerre expansion of kernels. *Ann. Biomed. Eng.* 21:573–589, 1993.

[27]Marmarelis, V. Z., K. H. Chon, Y. M. Chen, D. J. Marsh, and N. H. Holstein-Rathlou. Nonlinear analysis of renal autoregulation under broadband forcing conditions. *Ann. Biomed. Eng.* 21:591–603, 1993.

[28]Mukkamala, R., J. M. Mathias, T. J. Mullen, R. J. Cohen, and R. Freeman. System identification of closed-loop cardiovascular control mechanisms: diabetic autonomic neuropathy. *Am. J. Physiol.* 276:R905–R912, 1999.

[29]Mullen, T. J., M. L. Appel, R. Mukkamala, J. M. Mathias, and R. J. Cohen. System identification of closed-loop cardiovascular control: effects of posture and autonomic blockade. *Am. J. Physiol.* 272:H448–H461, 1997.

[30]Rechtschaffen, A., and R. Kales. A Manual of Standardized Terminology, Techniques and Scoring System for

Sleep Stages of Human Subjects. Los Angeles: BIS/BRI, UCLA, 1968.
[31]Rissanen, J. Estimation of structure by minimum description length. *Circ. Syst. Signal Process.* 1(3–4):395–406, 1982.
[32]Shepard, J. W. Hypertension, cardiac arrhythmias, myocardial infarction, and stroke in relation to obstructive sleep apnea. *Clin. Chest Med.* 3:437–458, 1992.
[33]Shiavi, R. Introduction to Applied Statistical Signal Analysis. Homewood, IL: Aksen Associates, 1991.
[34]Somers, V. K., M. E. Dyken, M. P. Clary, and F. M. Abboud. Sympathetic neural mechanisms in obstructive sleep apnea. *J. Clin. Invest.* 96:1897–1904, 1995.
[35]Vanninen, E., A. Tuunainen, M. Kansanen, M. Uusitupa, and E. Lansimies. Cardiac sympathovagal balance during sleep apnea episodes. *Clin. Physiol.* 16:209–216, 1996.
[36]Westwick, D. T., and R. E. Kearney. Nonparametric identification of nonlinear biomedical systems, Part 1: theory. *Crit. Rev. Biomed. Eng.* 26:153–226, 1998.
[37]Wiklund, U., B. O. Olofsson, K. Franklin, H. Blom, P. Bjerle, and U. Niklasson. Autonomic cardiovascular regulation in patients with obstructive sleep apnea: a study based on spectral analysis of heart rate variability. *Clin. Physiol.* 20:234–241, 2000.
[38]Yip, K. P., N. H. Holstein-Rathlou, and D. J. Marsh. Chaos in blood flow control in genetic and renovascular hypertensive rats. *Am. J. Physiol.* 261:F400–F408, 1991.
[39]Zwillich, C. W. Sleep apnoea and autonomic function. *Thorax* 53:S20–S24, 1998.